TENSION BUCKLING IN MULTILAYER ELASTOMERIC ISOLATION BEARINGS

James M. Kelly and Shakhzod M. Takhirov

TENSION BUCKLING IN MULTILAYER ELASTOMERIC ISOLATION BEARINGS

JAMES M. KELLY AND SHAKHZOD M. TAKHIROV

Seismic isolators are constructed from multiple layers of elastomer (usually natural rubber) reinforced with steel plates; they are, therefore, very stiff in the vertical direction, but soft in the horizontal direction. The buckling of these bearings under compression load is a well-understood phenomenon and has been widely studied. It is therefore unexpected that the buckling analysis for compression predicts that the isolator can buckle in tension at a load close to that for buckling in compression. The linear elastic model that leads to both compression and tension buckling is an extremely simple one, so it might be argued that the tensile buckling may be an artifact of the model itself rather than a property of the isolator. To test the simple theoretical model we have conducted a numerical simulation study using a finite element model of a multilayer elastomeric bearing. We find that the prediction of tensile buckling by the simple linear elastic theory is indeed accurate and not an artifact of the model.

1. Introduction

Seismic isolation using multilayer elastomeric isolators has been used in the United States and around the world for more than 20 years. The isolators are constructed from many layers of elastomer reinforced with steel shims, and are very stiff in the vertical direction, but soft in the horizontal direction. This enables them to carry the weight of a building, but cause the building to have a fundamental natural frequency that is both lower than that of the same building, if conventionally founded, and the dominant frequencies of strong ground motion.

They appear to be very stable, though the low shear stiffness causes a buckling phenomenon. However, it is straightforward to design them to have a large safety factor against buckling. The buckling of these bearings under compression load is a well-understood phenomenon, and has been widely studied. Buckling theory is based on a linearly elastic analysis. Although the elastomer is not really linearly elastic, the deformation is predominantly one of shear, and typical elastomers used in bearings are very close to linear over a large range of shear strain. While approximate, the linear theory is relatively accurate and adequate for most design purposes.

However, buckling analysis for compression has been used to make an unexpected prediction that the isolator can buckle in tension at a load close to that for buckling in compression. Of course, there are many examples of strange systems that buckle in tension, but these are entirely pathological in that the tension forces are always transferred to compression elements that produce the instability. This is not the case here. The buckling process is in fact tensile. The linear elastic model that leads to both compression and tension buckling is an extremely simple one, so it might be argued that tensile buckling may be an artifact of the model itself and not of the isolator.

For this reason we had undertaken a numerical simulation study using a finite element model of a multilayer elastomeric bearing to check whether the prediction of tensile buckling by the simple linear elastic theory is, in fact, accurate. We found this to be the case. The essential point is that the mechanics of the isolator in tension are the mirror image of that for the isolator in compression. In particular, when the isolator is in compression below the buckling load but laterally displaced, the layers in the center experience rotations that give the vertical load a component along the layer causing a shear deformation. In tension, the layers in the center experience rotations in the opposite direction giving a shear deformation due to the tensile force that permits the top of the isolator to move upwards by a much larger displacement than that which could be sustained in pure tension with no lateral displacement.

While the bearings are normally in compression, base-isolated tall buildings in near-fault locations can lead to situations where peripheral bearings in the isolation system can be required to take some amount of tension. This tension is caused by global overturning of the building produced by the lateral inertial force at the center of the mass of the isolated building. The maximum inertial force and the resulting maximum overturning movement occur at the same time as the maximum lateral displacement of the isolators; at first sight this would seem to be a critical situation. The value of the buckling analysis is that it demonstrates that the condition of the isolator in tension and shear is not as dire as had been feared. In tension, the layers in the center experience a rotation which allows a shear deformation caused by the tensile force and permits the top of the isolator to move upwards by a much larger displacement than that which could be sustained in pure tension with no lateral displacement. Thus the simultaneous occurrence of tension and shear in the isolator prevents the development of damage due to cavitation.

2. Overview

Earliest theoretical approaches to study the stability of rubber bearings by Haringx [1948; 1949a; 1949b] were based on linearity of the rubber material and small displacements. Theoretical predictions of the decrease in horizontal stiffness with increasing axial load based on Haringx's theory were made by Gent [1964] and Derham and Thomas [1981]. Simo and Kelly [1984] used finite element modeling to study the variation of lateral load-displacement behavior under increasing axial load.

An extensive experimental study of low shape factor elastomeric isolators used for base isolation was given by Aiken et al. [1989]. Buckling tests were conducted on doweled bearings; they consisted of applying monotonically increasing axial load to a bearing with the top of the bearing free to displace in the horizontal direction. The tests showed that the analytical formula gives a higher value of the critical load than the experimentally measured one.

Roeder et al. [1987] and Stanton et al. [1990] studied the stability of laminated elastomeric bearings experimentally and theoretically with due consideration given to axial shortening. Buckle and Kelly [1986] studied the stability of elastomeric bearings using a model bridge deck tested using a shaking table. Since the bearings were doweled, bearing overturning or rollover was clearly evident in these tests. Koh and Kelly [1986; 1988; 1989] developed a viscoelastic stability model and a mechanical model based on bearing test results. A comprehensive study of the basic theory and its application to design issues, including the stability problem, was presented by Kelly [1997].

Experimental determination of critical buckling behavior of steel-reinforced bearings at high shear strain was conducted by Buckle and Liu [1994]. Studies by Nagarajaiah and Ferrell [1999] introduced

a nonlinear analytical model based on the Koh–Kelly model and included large displacements, large rotations, and nonlinearity of the rubber. The model was verified through experimental results. Further experimental work on the stability of elastomeric bearings was presented by Buckle et al. [2002]. It was shown that the critical buckling load decreases with increasing horizontal displacement or shear strain. Finite element analysis results conducted on a plane model of the bearings with a coarse mesh were compared with the experimental results.

Some results on finite element analysis of the multilayered elastomeric bearings can be found in several papers and reports; see, for example, [Takayama et al. 1992].

3. Formulation of elementary stability theory of multilayer elastomeric isolators

The elementary theory for the buckling of isolation bearings treats the bearing as a continuous homogeneous beam in which plane sections normal to the undeformed axis remain plane but not necessarily normal to the deformed axis. The deformation is defined by three functions $u(x)$, $v(x)$, $\psi(x)$, which are the axial and lateral displacements of the centroidal axis and the rotation of a section normal to the undeformed axis, respectively. The overall shear deformation $\gamma(x)$ of the section is the difference between the rotations of the centroidal axis and the section, namely, $\gamma(x) = v'(x) - \psi(x)$.

The internal forces on the deformed plane section are the axial load $N(x)$ normal to the section, the shear force $V(x)$ parallel to the section and the bending moment $M(x)$, as shown in Figure 1. These internal forces are related to the deformation quantities through

$$N(x) = E_c A_s u'(x), \qquad V(x) = G A_s (v' - \psi), \qquad M(x) = E I_s \psi'(x).$$

A_s is the cross sectional area A increased by h/t_r, where h is the total height of the bearing (rubber plus steel), t_r is the total thickness of rubber. and E_c is the compression modulus of the bearing. The value of E_c for a single rubber layer is controlled by the shape factor $S =$(loaded area)/(force-free area), which is a dimensionless aspect ratio of a single layer of the elastomer. For example,

$$S = \begin{cases} S = b/t, & \text{infinite strip of width } 2b \text{ with a single layer thickness } t, \\ S = R/2t, & \text{circular pad of diameter } R \text{ and thickness } t, \\ S = a/4t, & \text{square of side } a \text{ and thickness } t. \end{cases}$$

In a circular isolator $E_c = 6GS^2$, while in the long strip isolator that will be used for the numerical simulation $E_c = 4GS^2$. The increase in the area is needed to account for the fact that the steel does not deform in the composite beam. I_s is the effective moment of inertia of the cross section. This is modified the same way as A. There is an additional modification to account for the fact that in the isolator the pressure distribution that generates the internal bending moment is a cubic parabola in contrast to regular beam theory where the bending stress distribution is linear. The effective bending stiffness, accounting for these two effects is [Kelly 1997]

$$EI_s = \begin{cases} \frac{1}{3} E_c I \frac{h}{t_r}, & \text{circular bearing,} \\ \frac{1}{5} E_c I \frac{h}{t_r}, & \text{strip bearing.} \end{cases}$$

Under the kinematic assumptions of this beam theory, the downward deflection of the top of the composite column representing the isolator and the resulting external work done by the applied load P are, respectively,

$$v(x) = \tfrac{1}{2} \int_0^h \left(2v'\psi - \psi^2\right)dx, \qquad W_{\text{ext}} = -Pv(x) = -\frac{P}{2} \int_0^h \left(2v'\psi - \psi^2\right)dx.$$

The internal stored energy of the column is given by

$$W_{\text{int}} = \tfrac{1}{2} \int_0^h N(x)u'dx + \tfrac{1}{2} \int M(x)\psi'(x)dx + \tfrac{1}{2} \int V(x)\big(v'(x) - \psi(x)\big)dx.$$

Application of the method of virtual work to the total work $W_{\text{int}} + W_{\text{ext}}$ with respect to the virtual displacements $\delta u(x)$, $\delta v(x)$, $\delta\psi(x)$ leads to the following set of equilibrium equations

$$N' = 0, \qquad V' - P\psi = 0, \qquad M' + V + P(v' - \psi) = 0. \tag{1}$$

The boundary conditions for Equations (1) are shown in Figure 1; the external loads applied to the column at $x = 0$ are the axial load P (or T), a transverse load H_o and a moment M_o.

From Equation (1)$_1$ we have $N = \text{const} = -P$. Integrating the second equation using the consistent boundary condition gives
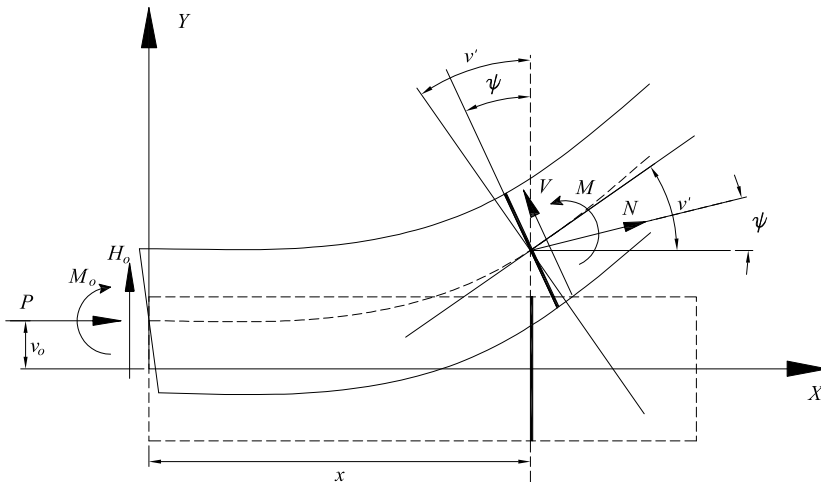
$$V - P\psi = -H_o, \tag{2}$$

and inserting $V = P\psi - H_o$ into the third equation gives $M' + Pv' = H_o$, which can be integrated to

$$M + Pv = M_o + Pv_o + H_o x, \tag{3}$$

where $v_o = v(0)$. These two integrated versions of equilibrium equations (2) and (3) are the starting point for the stability analysis of the isolator. When the constitutive equations are included, these become

$$EI_s\psi' + Pv = Pv_o + M_o + H_o x, \qquad GA_s(v' - \psi) - P\psi = -H_o.$$

Figure 1. Geometry and loads in theoretical study of buckling.

The second equation above can be used in two ways to give a pair of uncoupled equations for v and ψ. First we can write ψ in terms of v in the form $\psi = (GA_s v' + H_o)/(GA_s + P)$, and substitute ψ' into the first equation to get

$$EI_s \frac{GA_s}{GA_s + P} v'' + Pv = Pv_o + M_o + H_o x. \tag{4}$$

We can also express v in terms of ψ as $v' = (P + GA_s)\psi/(GA_s) - (H_o)/(GA_s)$, which, when substituted into the first, leads to

$$EI_s \frac{GA_s}{GA_s + P} \psi'' + P\psi = H_o. \tag{5}$$

Thus, Equations (4) and (5) for two kinematic variables have similar form, but different right hand sides. The most general form of solution, taking into account the connections between v and ψ, is

$$v = A\cos\alpha x + B\sin\alpha x + v_o + \frac{M_o}{P} + \frac{H_o}{P}x, \qquad \psi = \alpha\beta B\cos\alpha x - \alpha\beta A\sin\alpha x + \frac{H_o}{P},$$

where A and B are constants of integration and α, β are given by

$$\alpha^2 = \frac{P(P + GA_s)}{EI_s GA_s}, \qquad \beta = \frac{GA_s}{P + GA_s}.$$

These equations are now used to predict the buckling behavior of a bearing in an isolation system. As shown in Figure 2, the isolator is constrained against displacement and rotation at the bottom, against rotation at the top, but is free to move laterally at the top, which give boundary conditions $v(0) = 0$, $\psi(0) = 0$, $\psi(0) = 0$, $H_o = 0$ leading to $\alpha h = \pi$. The deformed configuration becomes

$$v(x) = \tfrac{1}{2}\delta_h\left(1 - \cos\frac{\pi x}{h}\right), \qquad \psi(x) = \tfrac{1}{2}\alpha\beta\delta_h\sin\frac{\pi x}{h}.$$
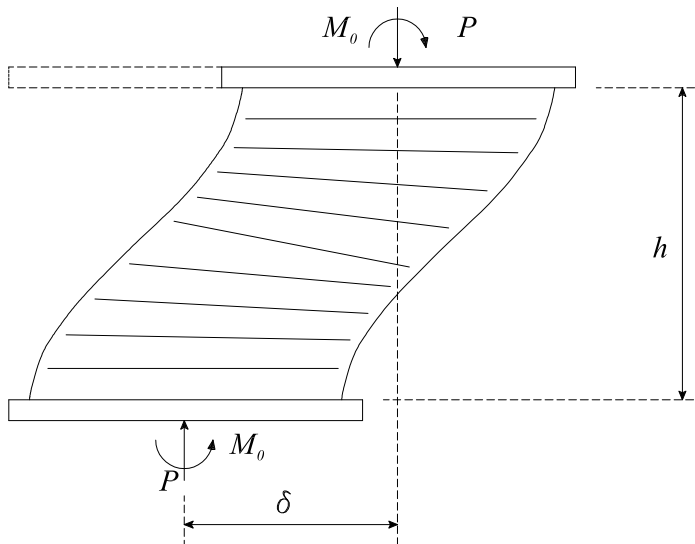
Figure 2. Boundary conditions for isolation bearing under a vertical load P. The bearing buckles with no lateral force constraint, but is prevented from rotating at each end.

The above result $\alpha^2 = \pi^2/h^2$ means that

$$\frac{P(P + GA_s)}{GA_s} = \frac{\pi^2 E I_s}{h^2} = P_E,$$

where P_E is the Euler load for the column without shear deformation. Denoting GA_s by P_S, the above equation for the buckling load can be recast as a quadratic $P^2 + PP_S - P_S P_E = 0$, which gives two critical loads: a compression load P_C and a tension load P_T

$$P_C = \frac{-P_S + \sqrt{P_S^2 + 4P_S P_E}}{2}, \qquad P_T = \frac{-P_S - \sqrt{P_S^2 + 4P_S P_E}}{2}. \tag{6}$$

For all reasonable values of the shape factor S, the P_S is so much less than P_E that it can be neglected, and the two critical loads can be approximated by

$$P_{C,T} = \pm\sqrt{P_S P_E}. \tag{7}$$

The significance of the tensile critical load becomes clear when we replace the generic load P in the formulae for α and β by $-T$, with the assumption $T \geq GA_s$, giving

$$\alpha^2 = \frac{T(T - GA_s)}{E I_s GA_s}, \qquad \beta = -\frac{GA_s}{T - GA_s},$$

showing that the buckled shape in tension $v(x)$ is the same as that in compression, but the rotation $\psi(x)$ is reversed, and the central layers of the bearing are rotated in the direction that facilitates the upward movement of the top through a rotated shear deformation. Because of the natural symmetry of shear, there is an intrinsic symmetry here between compression and tension.

## 4. Modification for change in length of column prior to buckling

One interesting aspect of the comparison between the buckling loads predicted by the theory and those obtained by the numerical simulation is the fact that while the theory has the buckling load in tension always slightly higher than that in compression for the same shape factor (the difference is GA_s), in the numerical results the buckling load in compression is always higher than that in tension. The reason for this is that theory neglects the change in length due to the axial load, whereas in the simulation when buckling is initiated, the bearing has shortened or lengthened. For smaller values of the shape factor, the changes in length can be significant.

Using the approximation $GA_s \ll P$ and the values of GA_s, $E I_s$ for a long strip bearing, the critical pressures $p_{\text{crit}} = P/A$ are given in the theoretical analysis by $p_{\text{crit}}/G = \pm 2\pi b S/(\sqrt{15}t_r)$, where t_r is the total thickness of rubber in the bearing. To compare the theory with the simulation we replace t_r by

$$t_r = t_r^o \left(1 \mp \frac{p_{\text{crit}}}{4GS^2}\right),$$

where the minus sign is for compression and the plus for tension. The buckling loads are then given by

$$\frac{p_{\text{crit}}}{G} = \pm \frac{2\pi b S}{\sqrt{15}t_r^o \left(1 \mp \dfrac{p_{\text{crit}}}{4GS^2}\right)}.$$
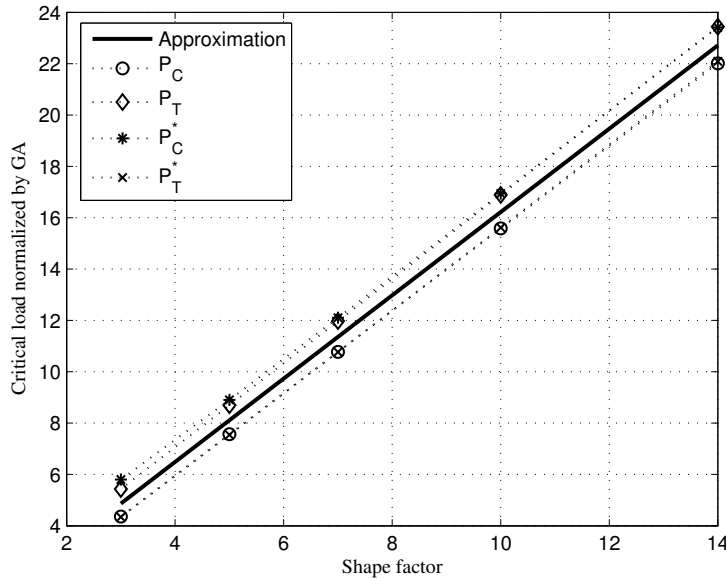
Figure 3. Theoretical buckling loads with and without global bearing deformation: Equation (6) versus (8); solid line corresponds to load approximation from (7).

Solving the last expression for p_{crit}/G and taking into account that $P = pA$ leads to

$$\frac{P^*_{C,T}}{GA} = \pm 2S^2 \left\{ 1 - \sqrt{1 \mp \frac{2\pi b}{St_r^0 \sqrt{15}}} \right\}. \tag{8}$$

Compression and tension critical loads computed by means of Equation (8) are presented in Figure 3.

It is easy to see that the value in compression is always larger than that in tension. The difference between $|P_{\text{crit}}/GA|$ in compression and tension is approximately $2(2\pi^2 b^2)/(15 t_r^{o\,2})$. For the case of the numerical models studied we have $b = t_r^o$. The difference is about $8/3$ and, thus, becomes less important with increasing S.

5. Numerical modeling of buckling in tension

In order to verify the tension buckling predicted by the simple analytical theory we use the general purpose finite element ABAQUS application [ABAQUS 2001] to model a steel-reinforced bearing and to study the buckling behavior in both tension and compression [Kelly and Takhirov 2004].

5.1. *Modeling details.* Five finite element models of a bearing are created. These numerical models have the same width and total rubber thickness, and steel shims have the same thickness also. The only difference between them is the shape factor of the bearing. The total thickness of rubber layers is the same in each model, but the thickness of a single rubber layer varies from model to model. The correspondence between the model name and the shim thickness is given in Table 1.

The finite element analysis on the elastomeric bearings is restricted to plane strain. The Oy-axis of the coordinate system is a vertical axis that extends across the steel shims and rubber layers, while the

Model	Steel shim thickness	Total rubber thickness	Width	Rubber layer thickness	Shape factor
Model 1	2.60	80.01	160.02	5.72	14
Model 2	2.60	80.01	160.02	8.00	10
Model 3	2.60	80.01	160.02	11.43	7
Model 4	2.60	80.01	160.02	16.00	5
Model 5	2.60	80.01	160.02	26.67	3

Table 1. Numerical models with various shape factors. All lengths in mm.

horizontal axis Ox corresponds to the lateral direction of the bearing as shown in Figure 4. Generally steel-reinforced rubber bearings have a hole in the middle of the steel plates and a rubber cover on the traction-free sides of the bearing. In order to create a model close to the theoretical one given earlier, the hole in the middle and the rubber cover are not included in the consideration.

In the analysis the end plates of the bearing are assumed to be undeformable. Therefore, in the numerical model, the top rubber layer of the bearing is connected to an absolutely rigid surface with the reference point in the middle at which the vertical load is applied. The bottom surface of the bearing is fixed. Two vertical sides of the bearing model are traction-free. The top surface is restrained against rotation around the Oz-axis (out of the plane), but is free to move horizontally.

Linearly elastic material properties are assumed for the steel plates with Young's modulus and Poisson's ratio equal to 200, 000 MPa and 0.3, respectively. Rubber materials have very little compressibility compared to their shear flexibility; these materials are usually modeled by a hyperelastic material model. ABAQUS [ABAQUS 2001] has a special family of hybrid elements to model the fully incompressible behavior seen in a rubber material. The following assumptions are made in modeling a rubber material: (1) elastic, (2) isotropic, (3) (almost) incompressible, and (4) includes nonlinear geometric effects.
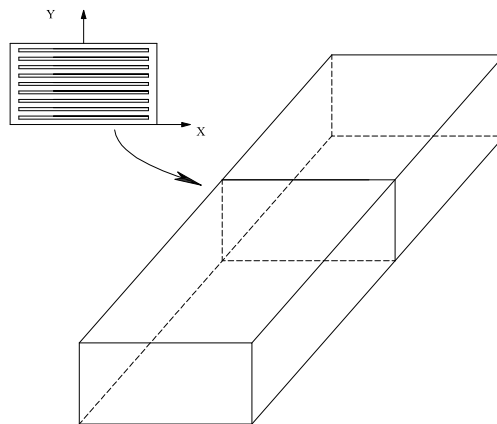
Figure 4. Geometry and coordinate axes of numerical simulation models.

Rubber model	C_{10}	C_{01}	C_{20}	C_{11}	C_{02}	D_1
Polynomial	193.4	−0.1	−0.8	0.2	0	0
neo-Hookean	345.0	0	0	0	0	9.7×10^{-7}

Table 2. Material parameters for two rubber models. C_{ij} in kPa, D_1 in kPa^{-1}.

Hyperelastic materials are described in terms of a strain energy potential U, which defines the strain energy stored in the material per unit of reference volume in the initial configuration as a function of the strain at that point in the material. The rubber is selected as a polynomial hyperelastic material of the second order. In this case, the strain energy potential has the form

$$U = \sum_{i+j=1}^{2} C_{ij}(I_1 - 3)^i (I_2 - 3)^j + \frac{(J^{\text{el}} - 1)^2}{D_1},$$

where C_{ij} and D_1 are the material parameters, I_1 and I_2 are the first and the second invariants of the deviatoric strain, and J^{el} is the elastic volume ratio.

Two rubber models are included in the consideration: a fully incompressible (polynomial) model, and an almost incompressible (neo-Hookean) model. The material parameters of the rubber can be expressed in terms of initial shear modulus G, and initial bulk modulus K via $G = 2(C_{10} + C_{01})$, $K = 2/D_1$. The values of the material parameters for both rubber models are presented in Table 2. Since D_1 is not equal to zero for the neo-Hookean model, this model allows some compressibility in the rubber material.

A supplemental study on the properties of the rubber models is conducted on a rubber cylinder and a rubber layer. The cylinder is used for the rubber material study in tension and compression. The layer, representing one single layer of the rubber locked between two rigid horizontal surfaces, is used to study behavior of the rubber material in shear with no vertical load. While both rubber materials are linearly elastic up to about 250% strain in shear, they exhibit a significant nonlinearity in tension or compression as shown in Figure 5.

5.2. *Critical buckling load in compression and tension.* The model is studied by a classical buckling analysis scheme available in ABAQUS. First the buckling mode of each bearing model is determined. Very small imperfections of about 1% of the steel layer thickness are introduced in the model; they are based on the buckling mode obtained in the buckling mode analysis. The postbuckling behavior is followed up to about 30% shear deformation.

The buckling analysis of the numerical bearing models reveals the following results. All models have significant horizontal drift caused by a large vertical load. The curves of the compression vertical load versus horizontal drift for all numerical models are shown in Figure 6. The critical buckling load increases with the increase in the shape factor. All plots show similar behavior with the majority of the change happening up to a 3% deformation after which they flatten out when the bearing is buckling. Figure 7 presents the corresponding curves of buckling in tension. The critical load is again dependent on the shape factor increasing with it. The buckling in tension is more sudden, so the point at which buckling begins moves very close to the vertical axis, and the shear when the buckling starts in tension
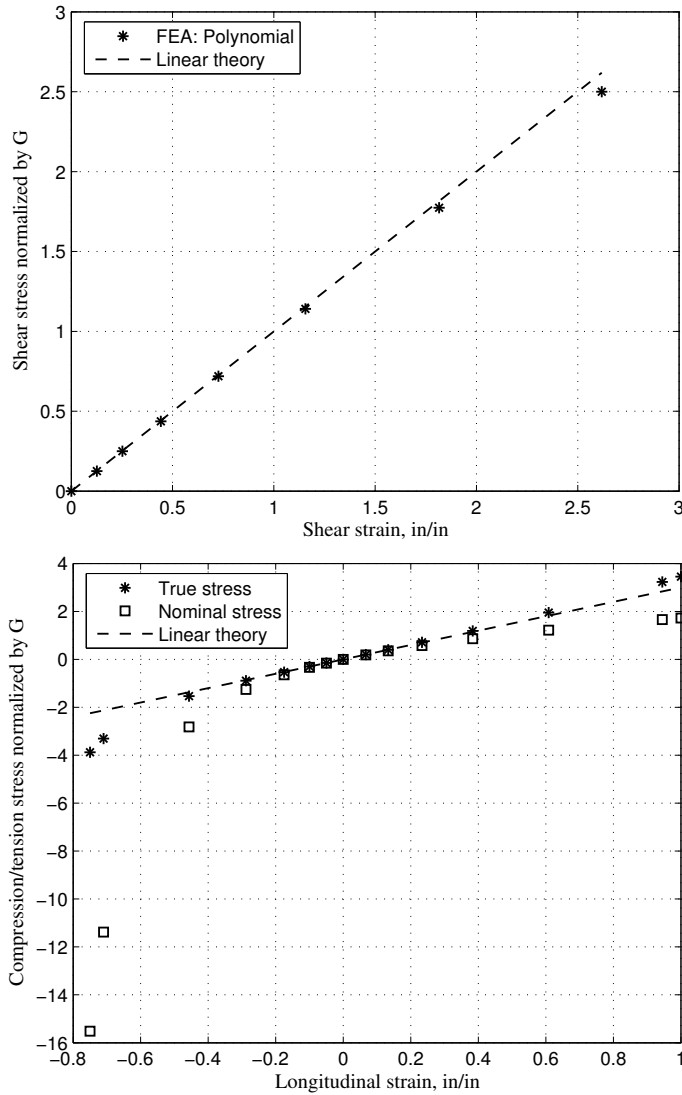
Figure 5. Properties of rubber material in (top) shear and (bottom) compression/tension deformation (polynomial rubber material).

can be as low as 0.2%; see Model 5 with the smallest shape factor. Increase in the shape factor moves this point closer to the 3% critical strain obtained for the compression buckling.

Theoretical critical force versus the shape factor for the corresponding numerical model was discussed earlier; see Figure 3. Theoretical buckling compression load is always less than the absolute value of the tension load for the simple theoretical solution presented in Equation (6), which is not consistent with the numerical analysis results shown in Figure 8. The critical load determined by Equation (8) takes into account shortening or elongation of the bearing in the vertical direction. Therefore, it correlates better with numerical results. As the latter show, the compression buckling load is always greater than the absolute value of the tension buckling load shown in Figure 8 by dashed and dot-dashed lines. Figure 8
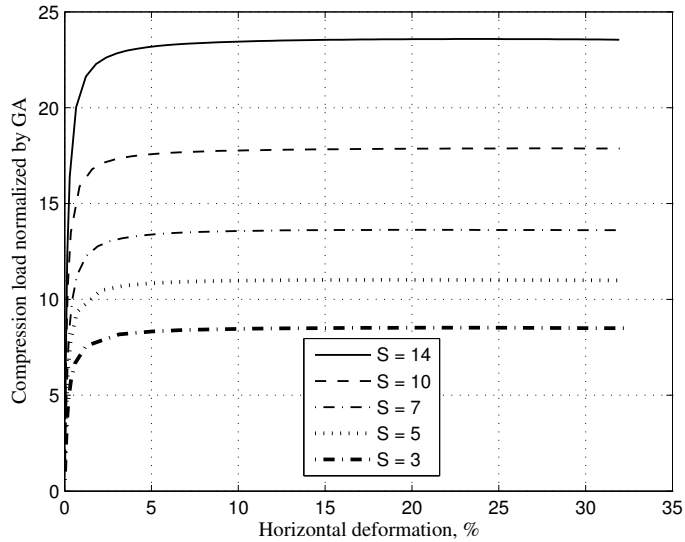
Figure 6. Buckling diagram for all models (compression).
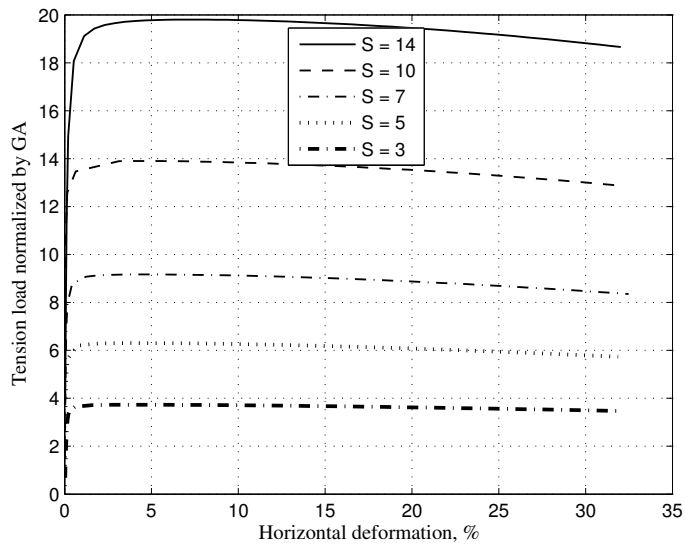
Figure 7. Buckling diagram for all models (tension).

also shows no significant differences between critical buckling load for incompressible (polynomial) and compressible (neo-Hookean) rubber materials. As a typical result, Figures 9–12 show deformed shapes of two numerical models in compression and tension.

The numerical results on buckling behavior of the bearing have satisfactory correlation with the theoretical solutions presented earlier. The theoretical study and the finite element analysis lead to the following conclusions. The critical buckling load increases with the shape factor; this behavior is almost
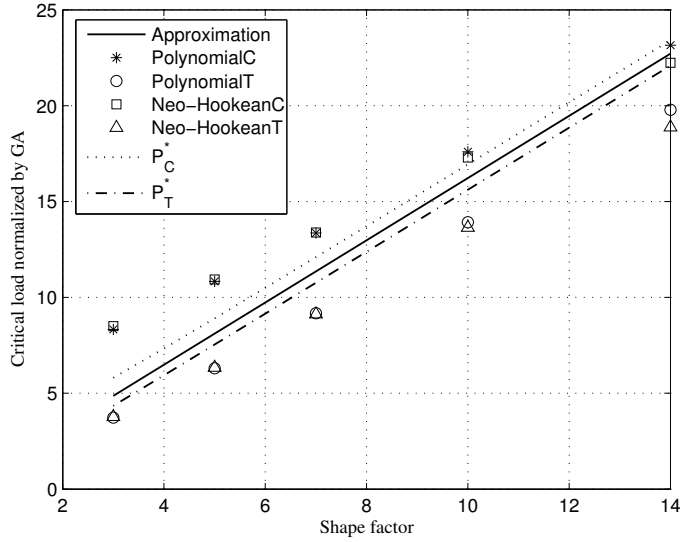
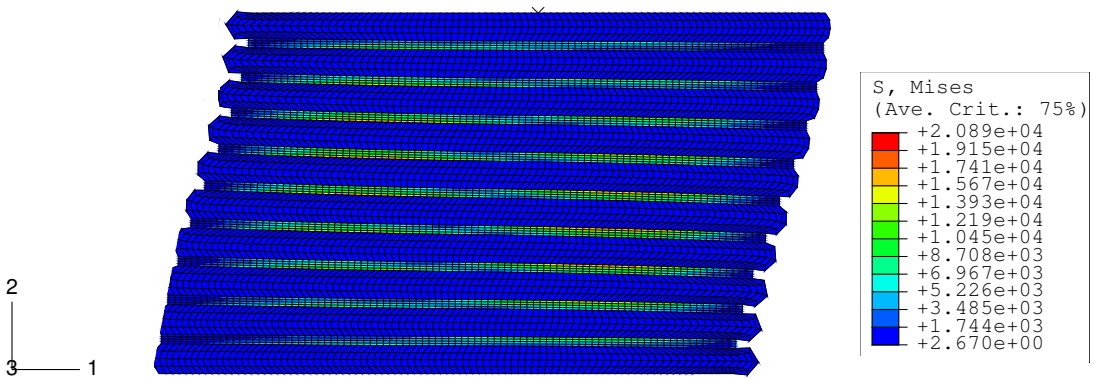**Figure 8.** Critical buckling load (normalized by GA) versus shape factor.
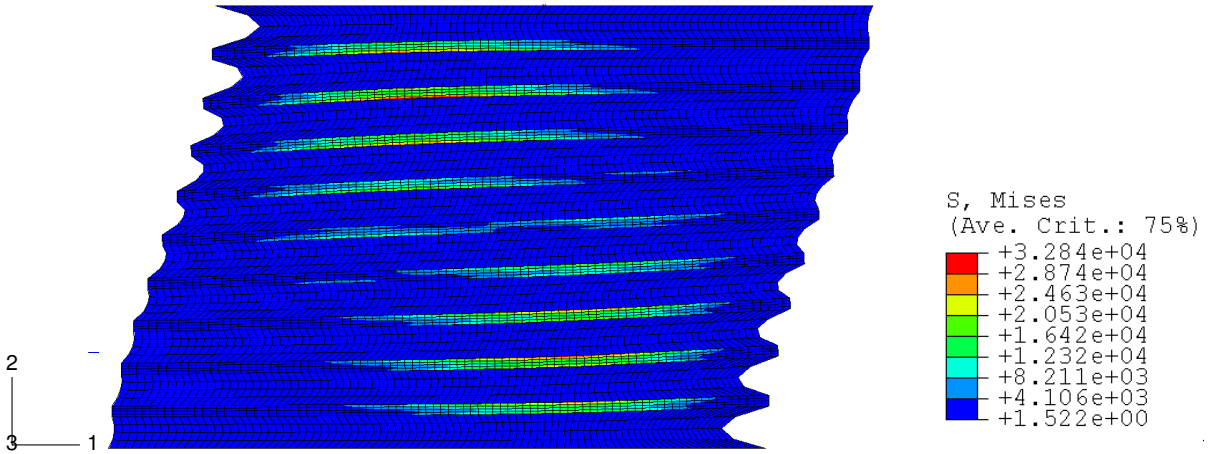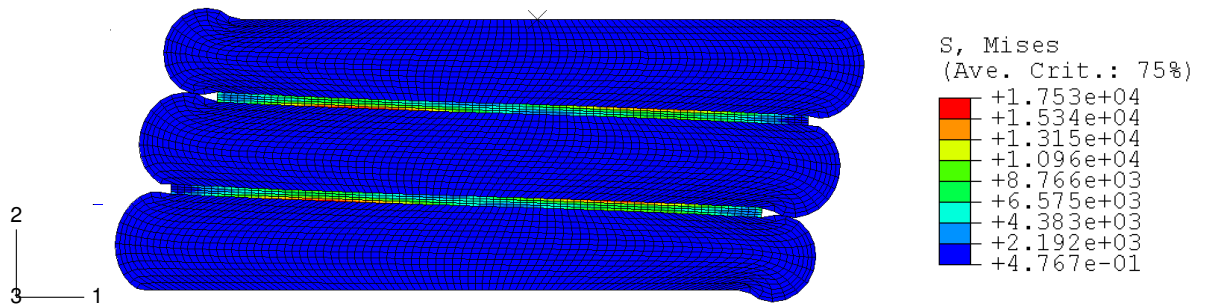

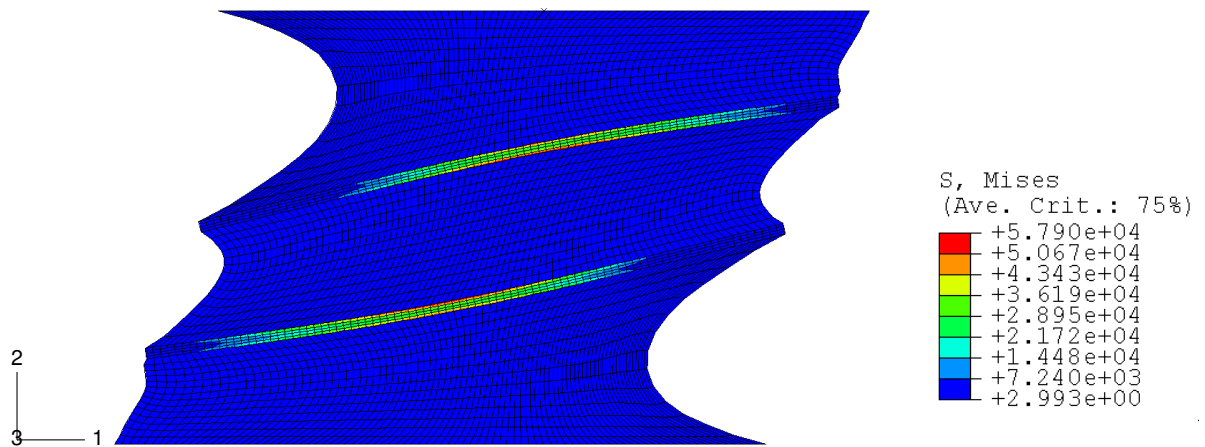**Figure 9.** Buckled shape and Mises stresses for Model 2 (compression).

linear as predicted by the theory. The numerical compression buckling load is almost always higher than the theoretically estimated one for all bearings. The compression buckling load is always higher than the absolute value of the corresponding tension load due to nonlinear geometry effects noted for the simple rubber cylinder model. The numerical models have different postbuckling behaviors in compression and tension. In compression, the vertical load remains almost the same after the buckling occurs, and the bearing deflects horizontally. In contrast, the vertical load in tension slowly decreases with horizontal deflection.

Figure 10. Buckled shape and Mises stresses for Model 2 (tension).

Figure 11. Buckled shape and Mises stresses for Model 5 (compression).

Figure 12. Buckled shape and Mises stresses for Model 5 (tension).

6. Conclusions

We have shown that numerical analysis confirms that the buckling of a bearing in tension is not an artifact of the way the theory has been set up. Of course, it must be acknowledged that a bearing will experience cavitation before the buckling load can be achieved. However, the theory shows that under high seismic loading, the isolators that experience tension will avoid the possibility of cavitation since the tension loading due to the overturning of the structure is accompanied by large lateral shear. Moreover, due to the interaction between shear and the vertical stiffness, the tension stresses are much less than they would be if the tension force were applied in the absence of shear.

It has been the purpose of this paper to demonstrate that the condition of the isolator in tension and shear is not as dire as has been feared. The analysis has shown that the mechanics of the isolator in tension are the mirror image of those for the isolator in compression. In particular, when the isolator is in compression below the buckling load but laterally displaced, the layers in the center experience a rotation which gives the vertical load a component along the layer and turns the compression displacement into a shear deformation. In tension the rubber layers in the center of the bearing experience a rotation in the opposite direction which allows a shear deformation caused by the tensile force and permits the top of the isolator to move upwards by a much larger displacement than that which could be sustained in pure tension with no lateral displacement. The elastomer can sustain only small strains in the state of triaxial stress generated by pure tension on a multilayer isolator with a large shape factor, but can sustain shear strains on the order of 500–600%. Thus the simultaneous occurrence of tension and shear allows the isolator to avoid the damaging effects of cavitation.

References

[ABAQUS 2001] *ABAQUS 6.2 user manual*, Version 6.2, Hibbitt Karlsson Sorensen Inc., Pawtucket, RI, 2001.

[Aiken et al. 1989] I. D. Aiken, J. M. Kelly, and F. F. Tajirian, "Mechanics of low shape factor elastomeric seismic isolation bearings", Technical report UCB/EERC-89/13, Earthquake Engineering Research Center, University of California, Berkeley, CA, 1989.

[Buckle and Kelly 1986] I. G. Buckle and J. M. Kelly, "Properties of slender elastomeric isolation bearings during shake table studies of a large-scale model bridge deck", pp. 247–269 in *Joint sealing and bearing systems for concrete structures*, vol. 1, American Concrete Institute, Detroit, MI, 1986.

[Buckle and Liu 1994] I. G. Buckle and H. Liu, "Experimental determination of critical loads of elastomeric isolators at high shear strain", *NCEER Bull.* **8**:3 (1994), 1–5.

[Buckle et al. 2002] I. Buckle, S. Nagarajaiah, and K. Ferrell, "Stability of elastomeric isolation bearings: experimental study", *J. Struct. Eng. ASCE* **128**:1 (2002), 3–11.

[Derham and Thomas 1981] C. J. Derham and A. G. Thomas, "The design of seismic isolation bearings", pp. 21–36 in *Control of seismic response of piping systems and other structures by base isolation*, Earthquake Engineering Research Center, University of California, Berkeley, CA, 1981.

[Gent 1964] A. N. Gent, "Elastic stability of rubber compression springs", *J. Mech. Eng. Sci.* **6**:4 (1964), 318–326.

[Haringx 1948] J. A. Haringx, "On highly compressible helical springs and rubber rods and their application for vibration-free mountings, I", *Philips Res. Rep.* **3** (1948), 401–449.

[Haringx 1949a] J. A. Haringx, "On highly compressible helical springs and rubber rods and their application for vibration-free mountings, II", *Philips Res. Rep.* **4** (1949), 49–80.

[Haringx 1949b] J. A. Haringx, "On highly compressible helical springs and rubber rods and their application for vibration-free mountings. III", *Philips Res. Rep.* **4** (1949), 206–220.

[Kelly 1997] J. M. Kelly, *Earthquake-resistant design with rubber*, 2nd ed., Springer, London, 1997.

[Kelly and Takhirov 2004] J. M. Kelly and S. M. Takhirov, "Analytical and numerical study on buckling of elastomeric bearings with various shape factors", Technical report UCB/EERC-2004/03, Earthquake Engineering Research Center, University of California, Berkeley, CA, 2004.

[Koh and Kelly 1986] C. G. Koh and J. M. Kelly, "Effects of axial load on elastomeric bearings", Technical report UCB/EERC-86/12, Earthquake Engineering Research Center, University of California, Berkeley, CA, 1986.

[Koh and Kelly 1988] C. G. Koh and J. M. Kelly, "A simple mechanical model for elastomeric bearings used in base isolation", *Int. J. Mech. Sci.* **30**:12 (1988), 933–943.

[Koh and Kelly 1989] C. G. Koh and J. M. Kelly, "Viscoelastic stability model for elastomeric isolation bearings", *J. Struct. Eng. ASCE* **115**:2 (1989), 285–302.

[Nagarajaiah and Ferrell 1999] S. Nagarajaiah and K. Ferrell, "Stability of elastomeric seismic isolation bearings", *J. Struct. Eng. ASCE* **125**:9 (1999), 946–954.

[Roeder et al. 1987] C. W. Roeder, J. F. Stanton, and A. W. Taylor, "Performance of elastomeric bearings", NCHRP Rep. 298, Trans. Res. Board, National Research Council, Washington, D. C., 1987.

[Simo and Kelly 1984] J. C. Simo and J. M. Kelly, "Finite element analysis of the stability of multilayer elastomeric bearings", *Eng. Struct.* **6**:3 (1984), 162–174.

[Stanton et al. 1990] J. F. Stanton, G. Scroggins, A. W. Taylor, and C. W. Roeder, "Stability of laminated elastomeric bearings", *J. Eng. Mech. ASCE* **116**:6 (1990), 1351–1371.

[Takayama et al. 1992] M. Takayama, H. Tada, and R. Tanaka, "Finite-element analysis of laminated rubber bearing used in base-isolation system", *Rubber Chem. Technol.* **65**:1 (1992), 46–62. Rubber Division, ACS.

JAMES M. KELLY: jmkelly@berkeley.edu
Earthquake Engineering Research Center, 1301 South 46th St., Bldg. 451, University of California, Berkeley, Richmond, CA 94804, United States

SHAKHZOD M. TAKHIROV: takhirov@berkeley.edu
Earthquake Engineering Research Center, 1301 South 46th St., Bldg. 451, University of California, Berkeley, Richmond, CA 94804, United States